Using multi-band InSAR data for detecting local deformation phenomena induced by the 2016-2017 Central Italy seismic sequence

Marco Polcari[1], Antonio Montuori[1], Christian Bignami[1], Marco Moro[1], Salvatore Stramondo[1], Cristiano Tolomei[1]

1. Istituto Nazionale di Geofisica e Vulcanologia, Via di Vigna Murata 605, 00143, Roma

Corresponding author: marco.polcari@ingv.it, +39 0651860619, Via di Vigna Murata 605, 00143 Rome, Italy

Abstract - In this work we exploit X- and C-band InSAR data for detecting local deformation phenomena induced by the 2016-2017 Central Italy seismic sequence. Our goal is to highlight the usefulness of multi-band InSAR analysis for Hazard assessing and Rapid Mapping purposes when *in-situ* investigations are difficult or dangerous to be performed. Indeed, local seismic-induced effects (such as landslides, avalanches, subsidence, etc.) could severely impact the environment and the population in the surrounding of areas hit by earthquakes. We focused on four areas, named *Monte Vettore*, *Podalla*, *Bolognola* and *Cicconi*, where InSAR outcomes revealed how the main seismic events of the sequence activated several landslides and secondary faults interested by deformation of ~2-3cm along the satellite Line-of-Sight (LoS). The use of multi-band InSAR data allows the observation of multi-scale deformation phenomena with both different spatial resolution and coverage, highlighting the limits and constraints of different SAR sensors. Moreover, it ensures the crosschecking of displacement patterns retrieved through different InSAR products, especially when no ground truth or *in situ* ancillary data are available for validation purposes. As a result, the retrieved InSAR information can support the Scientific Community and the Institutions in the management of crisis emergencies.

Keywords - 2016-2017 Central Italy seismic sequence, SAR Interferometry, Local seismic-induced effects, Deformation phenomena, Hazard assessement

INTRODUCTION

The 2016-2017 Central Italy seismic sequence has been a long sequence consisting of more than 60 earthquakes with magnitudes greater than Mw 4.0 spanning from August 2016 to January 2017. Because of the density of villages and towns as well as the persistence and concentration in the same Central Appenine area, the impact of the sequence on population and buildings was highly devastating. It caused more than 300 casualties and many buildings were destroyed or severely damaged, such as in Accumuli and Amatrice villages (Masi et al., 2016). Also the historical-artistic heritage of the area was affected by the earthquakes, which for example caused the collapse of the Basilica of San Benedetto and the Co-Cathedral of Santa Maria Argentea in Norcia and the Sant'Agostino church in Amatrice.

The sequence we have analyzed consists of 4 mainshocks characterized by a normal fault mechanism and located among Marche, Umbria, Lazio and Abruzzo regions (http://cnt.rm.ingv.it/): the Mw 6.0 Amatrice earthquake occurred on August 24th 2016 (Bignami et al., 2016; Cheloni et al., 2016), the Mw 5.9 Visso earthquake occurred on October 26th 2016, the Mw 6.5 Norcia earthquake occurred on October 30th 2016 (Cheloni et al., 2017), and the Mw 5.5 Montereale earthquake occurred on January 18th 2017. Many foreshocks and aftershocks (with Mw even greater than 5.0) were also observed during this temporal span. The four mainshocks have been located at a depth of ~10 Km in an area of ~ 70 Km of extension (http://cnt.rm.ingv.it/). Because of the relatively shallow depth of the earthquakes, they produced significant surface deformation fields, reaching up to ~70 cm of ground displacement (e.g. the Norcia earthquake), as clearly highlighted by Synthetic Aperture Radar Interferometry (InSAR) data (Figure 1). The capability of InSAR data in constraining the co-seismic deformation induced by seismic events was extensively demonstrated by considering both large scale earthquakes (Chini et al., 2010; Massonnet et al., 1993) and smaller scale events (Polcari et al., 2016; Stramondo et al., 2014). Nowadays, SAR systems operating at different frequencies are included in Earth Observation (EO) programs of several space agencies for risk mitigation purposes, such as the L-band ALOS-2 mission of the Japan Aerospace eXploration Agency (JAXA), the C-band Sentinel-

1 (S1) mission from the European Space Agency (ESA) and the X-band COSMO-SkyMed (CSK) mission of the Italian Space Agency (ASI). Therefore, depending on the scale of the observed phenomenon, it is possible to exploit L- (1 – 2GHz), C- (4 – 8 GHz) or X-band (8-12GHz) SAR data. In Figure 1, the displacement maps due to the Amatrice, Visso, Norcia and Montereale earthquakes are estimated by the L-band ALOS-2 SAR data. Thanks to its long wavelength (λ ~24cm), the L-band SAR data are less affected by temporal decorrelation problems. Moreover, using X- and C-band data, an occurred large surface displacement could lead to coherence loss and unwrapping phase errors, especially in proximity of the deformation peak and fault location. However, besides the large co-seismic deformations, the long seismic sequence further induced several local deformation phenomena, such as landslides or avalanches (Emergeo W.G., 2016). Although considered "secondary effects" induced by earthquakes, these local phenomena severely impact the interested areas, causing dangerous landscape and structural changes, thus increasing the risk for the surrounding villages, inhabitants and critical infrastructures (e.g. dams, bridges). They can provide non-negligible losses in terms of human life, building damages, environmental instabilities, transport facilities and financial resources. As a result, an effective InSAR-based monitoring strategy could be suitable not only to detect and monitor such phenomena at local scales, but also to provide useful information for the seismic risk mitigation of the affected areas in short and medium terms.

The aim of this paper is to investigate such local effects by means of X- and C-band InSAR data, exploiting the different sensors characteristics on the base of resolution and the orientation of the phenomenon with respect to the geometry of the satellite Line-of-sight (LoS). The scale of the investigated phenomena is generally few centimeters, then the X- (λ ~3.1cm) and the C-band (λ ~5.6cm) SAR data are the only able to image them. These dual band InSAR data confirmed to be suitable and very useful in detecting the "secondary effects" of an earthquake, especially when the complex and rugged topography makes complicated the *in-situ* analysis.

In this work, the attention was focused on 4 case studies located in the surroundings of the epicenters, respectively the *Monte Vettore*, *Bolognola*, *Podalla* and *Cicconi* sites. They were selected since InSAR data revealed localized deformations occurring after the main events of the seismic sequence. Hence, they are interesting to study and monitor for security and safeguarding purposes.

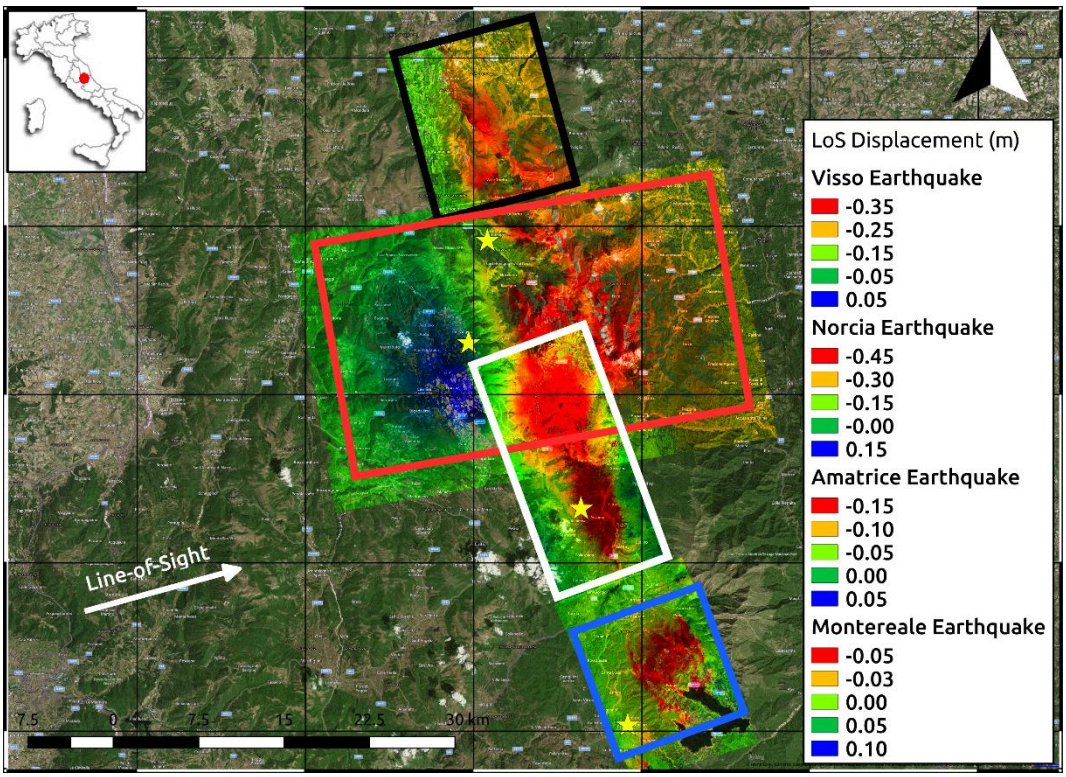

Figure 1: InSAR LoS overall displacement induced by the 2016-2017 Central Italy seismic sequence. The map was retrieved by L-band ALOS-2 ascending SAR data. From north to south, the displacement fields due to the Visso (black rectangle), Norcia (red rectangle), Amatrice (white rectangle) and Montereale (blue rectangle) earthquakes are shown, respectively. In the same order, the epicenters are indicated as yellow stars. The different color scales used for the displacement range values are due to the different magnitude of seismic events.

SEISMOTECTONIC FRAMEWORK AND GEOLOGICAL SETTING

Since Neogene geologic period, the Central Apennine chain developed as an east-verging fold and thrust belt, (Bally et al., 1988) accreted in consequence of the contemporaneous flexural-hinge retreat of the Adria plate and the back-arc opening of the Tyrrhenian basin (Meletti et al., 2000 and references therein). This portion of Apennines is characterized by the superposition of two main tectonic phases, evidenced by the presence of a complex pattern of thrusts, strike-slip faults, folds and normal faults (Barchi et al., 1998; Lavecchia et al., 1994; Tavarnelli, 1999). The first compressional phase took place during the Upper Miocene-Lower Pliocene and is responsible for the formation of the E-NE

verging fold and thrust belt. The second and latter phase superimposed during the Upper Pliocene and Quaternary, generating extensional basins bounded by NW-SE to N-S trending normal faults.

The present-day NE trending extensional stress field revealed by geodetic data (D'Agostino et al., 2011; Devoti et al., 2011), focal mechanisms (Chiarabba et al., 2009) and borehole breakout (Mariucci et al., 2010), is related to the persistence of back-arc extension, with deformation occurring on active normal faults NW-SE trending, SW-dipping. Active extension, earthquakes and evidence of active faulting are mainly concentrated along the axial belt, close to the main topographic ridge, where the strongest historical (Intensity = XI) and instrumental seismicity (M > 5.8) occurs (Barchi et al., 2000 and reference therein).

From a geological point of view, the observed phenomena described below are located in a portion of the Umbria-Marche Apennines known as Inner Ridge (Lavecchia & Pialli, 1980; Scarsella, 1951), a carbonate multilayer sequence constituted by rift and passive margin environment sediments. This stratigraphic sequence is represented by a Lower Liassic massive carbonate platform (Calcare Massiccio fm), superimposed by Middle Lias-Middle Eocene pelagic sequence of cherty limestones (Corniola fm, Calcari Diasprigni fm, Maiolica fm, Scaglia Bianca fm, Scaglia Rossa fm) and marly formations (Rosso Ammonitico fm, Marne a Fucoidi fm, Scaglia Variegata fm, Scaglia Cinerea fm).

X- AND C-BAND DATA

The SAR data adopted in this study were acquired by the CSK and S1 missions (Table 1). The choice to use CSK and/or S1 data relies on the scale, the size and the spatial extension of the phenomena to observe. S1 uses a wavelength of 5.66cm (f=5.33 Ghz) and the SAR data are characterized by a pixel posting of ~3x15m in the Interferometric Wide Swath (IW) acquisition mode. This is a new form of ScanSAR imaging, namely the Terrain Observation with Progressive Scan SAR (TOPSAR), that acquire data in burst mode by cyclically switching the antenna beam between 3 adjacent sub-swaths. Therefore, the S1 missions are mainly designed to cover large areas (~250Km) with revisit time of 6 days, thus allowing to significantly reduce the temporal decorrelation induced by the presence of

snow, vegetated area, etc. On the other hand, the CSK X-band SAR data are more affected by temporal decorrelation effects due to the smaller wavelength, λ=3.1cm (f=9.6Ghz). The latter could also lead to phase ambiguity problems in the study of large surface deformation fields, since an entire phase cycle represents a LoS displacement of 1.55cm, i.e. $\lambda/2$, instead of 2.83cm for the C-band data. However, the ~2x2m pixel posting provided in the CSK StripMap acquisition mode allows to obtain more details about the observed area and improves the analysis of small scale deformation phenomena. All the SAR data used in this work were processed by GAMMA© SAR software (Werner and Wegmuller, 1997), a commercial software developed by the Swiss corporation GAMMA© Remote Sensing Research and Consulting AG. It is mainly designed for the SAR interferometric processing chain and allows a useful checking of the data processing adopting a step-by-step strategy. In the following, InSAR data processing details for each case study are reported.

<u>Monte Vettore</u>

4 CSK data, acquired along descending orbit, were exploited to image the pre-seismic, the co-seismic and the post-seismic deformations, induced by the 6.0 Mw Amatrice earthquake occurred on August 24th 2016. The SLC images were acquired on July 3rd, on August 20th and 28th, and on September 1st 2016, respectively. The 30m (1-arcsecond) Shuttle Radar Topography Mission (SRTM) digital elevation model (DEM) (https://lta.cr.usgs.gov/SRTM1Arc) was used to remove the topographic contribution. Then a multi-look factor of 15x15 were applied to the CSK data in the range and azimuth directions, in order to obtain a ~30x30 meters pixel posting. Three interferograms capturing all the phases of the seismic cycle (pre-, co- and post-seismic) were estimated. In order to increase the coherence, they were filtered with the Goldstein filtering (Goldstein and Werner, 1998). Because of the high sensitivity of the X-band data to the decorrelation effects, a quite strong data filtering was applied by setting the exponent parameter and the windows size values of the Goldstein filtering to 0.8 and 32, respectively. This choice allowed to preserve the details of the observed scenario, mitigating the effects of coherence loss at X-band. The minimum cost flow (MCF) algorithm

(Costantini, 1998) was used for the phase unwrapping step.

Bologna

The Northern Sector of the Mount Sibillini, close the town of Bolognola, was analyzed by CSK and S1 SAR data acquired along descending orbit, with the aim of investigating the effects induced by the Visso and Norcia earthquakes. They occurred on October 26th and 30th 2016 with the respective epicenters located at ~10 Km one from each other. The CSK dataset consists in a pair of SLC data acquired on October 23rd and 31th 2016. In order to preserve the high resolution of CSK SAR data, the topographic contribution was removed by a 10m TINITALY DEM. Then, the data were multi-looked by factors 5x5 resulting in a ~10m pixel posting along range and azimuth directions. The retrieved interferogram was filtered by Goldstein filter (Goldstein and Werner, 1998), using the same parameters chosen for the *Monte Vettore* case study. Then, it was unwrapped with the MCF algorithm (Costantini, 1998). On the other hand, S1 SAR data were acquired on October 26th 2016, before the Visso earthquake, and on November 1st 2016. The 30m SRTM DEM was used to remove the topography and the S1 data were multi-looked to have the same pixel posting of SRTM product (multi-look factors 8x2). Since the S1 (C-band) data show higher coherence than the CSK (X-band) ones, a slightly weaker Goldstein filtering (Goldstein and Werner, 1998) was adopted by setting the exponent parameter and the windows size values to 0.6 and 16, respectively. Then, the same processing steps for the CSK interferogram were applied.

Podalla

The InSAR investigation concerning the Deep-Seated Gravitational Slope Deformation (DGSD) of Podalla, in the proximity of the Fiastra Lake dam, was conducted by means of two pairs of S1 descending data. The first pair was acquired on August 21st and 27th 2016, whereas the second one was acquired on October 25th and 31st 2016. Therefore, the effects of both the Mw 6.0 Amatrice earthquake and the Mw 5.9 Visso plus the Mw 6.5 Norcia earthquakes were simultaneously imaged. The 30m SRTM DEM was exploited to remove the topography. The Goldstein filtering step

(Goldstein and Werner, 1998) was performed by using the same settings used for the S1 data in the *Bolognola* case (exponent parameter equal to 0.6 and windows size equal to 32). Finally, both the interferograms were unwrapped by using the MCF phase unwrapping algorithm (Costantini, 1998).

Cicconi

This area, located about 3Km NW from the Fiastra municipality, was observed by using 4 SLC data provided by S1-A and S1-B missions as well as one CSK pair data. The S1 data were acquired along ascending orbit on October 15th, 21st and 27th and on November 2nd 2016, respectively. Three interferograms were calculated, corresponding to the pre-seismic, co-seismic and post-seismic period of the Mw 5.9 Visso mainshock, respectively. The S1 data were multi-looked by factors 8x2 along range and azimuth direction, resulting in a pixel posting of ~30x30m. The 30m SRTM DEM was used to remove the topography and the same processing parameters used in the *Podalla* case were applied to estimate the two interferograms. On the other hand, the CSK interferogram was estimated by two images acquired along ascending orbit on October 21st and 30th 2016 (just before the Norcia event). As for the *Bolognola* case study, the topographic contribution was removed through the 10m TINITALY DEM and the data were multi-looked by factors 5x5, resulting in a ~10m pixel posting along both the range and azimuth directions. The retrieved interferogram was filtered by Goldstein filtering approach (Goldstein and Werner, 1998) following the same criteria adopted for CSK data in the previous cases. Finally, the MCF algorithm (Costantini, 1998) was used for the unwrapping step.

Table 1: used SAR dataset

AREA	DATE1	DATE2	MISSION	ORBIT	INCIDENCE ANGLE (°)	BASELINE (m)
Monte Vettore	20160703	20160820	CSK	D	33.98	93
	20160820	20160828	CSK	D	33.98	101
	20160828	20160901	CSK	D	33.98	315
Bolognola	20161023	20161031	CSK	D	33.98	277
	20161026	20161101	S1	D	39.19	78
Podalla	20160821	20160827	S1	D	43.8	75
	20161025	20161031	S1	D	33.8	95
Cicconi	20161015	20161021	S1	A	33.5	119
	20161021	20161027	S1	A	33.5	70
	20161027	20161102	S1	A	33.5	21
	20161021	20161030	CSK	A	29.5	385

RESULTS: INDUCED PHENOMENA

Mt. Vettore

The CSK InSAR outcomes highlighted a deformation signal on the Mt. Vettore flank, strictly connected to the co-seismic phase of the Mw 6.0 Amatrice earthquake. Indeed, as showed in Figures 2-A and 2-C, there are no significant ground movements in the area for both pre-seismic and post-seismic phases. On the other hand, the co-seismic phase interferogram reveals two distinct patterns of displacement. One is visible in the bottom left corner of Figure 2B, and it is due to the dislocation caused by the main fault that ruptured on August 24th (Bignami et al., 2016). The second pattern is highlighted by the blue rectangle in Figure 2B, where the displacement lays along the SW flank of Mt. Vettore peaking at ~12cm along the satellite LoS. As shown in the zoom of Figure 3, it occurs along a ~5Km long continuous fracture on the flank (also revealed by ground surveys) and is most probably due to the combination of tectonic effects and gravitational phenomena (Albano et al., 2016).

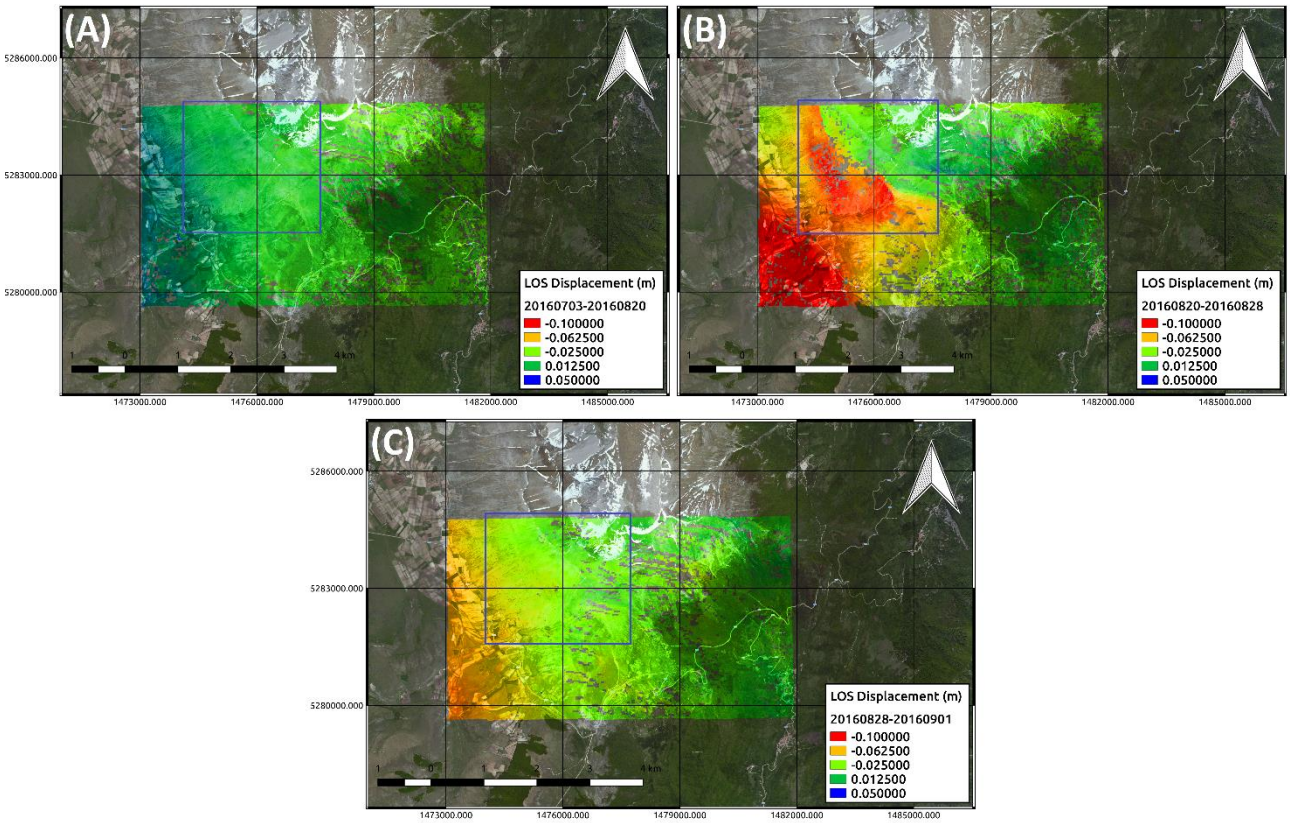

Figure 2: InSAR maps highlighting the effects of the pre-seismic (A), co-seismic (B) and post-seismic (C) phase of the August 24th 2016 Mw 6.0 Amatrice earthquake for the Mt. Vettore. Blue rectangle highlights the area interested by the detected deformation.

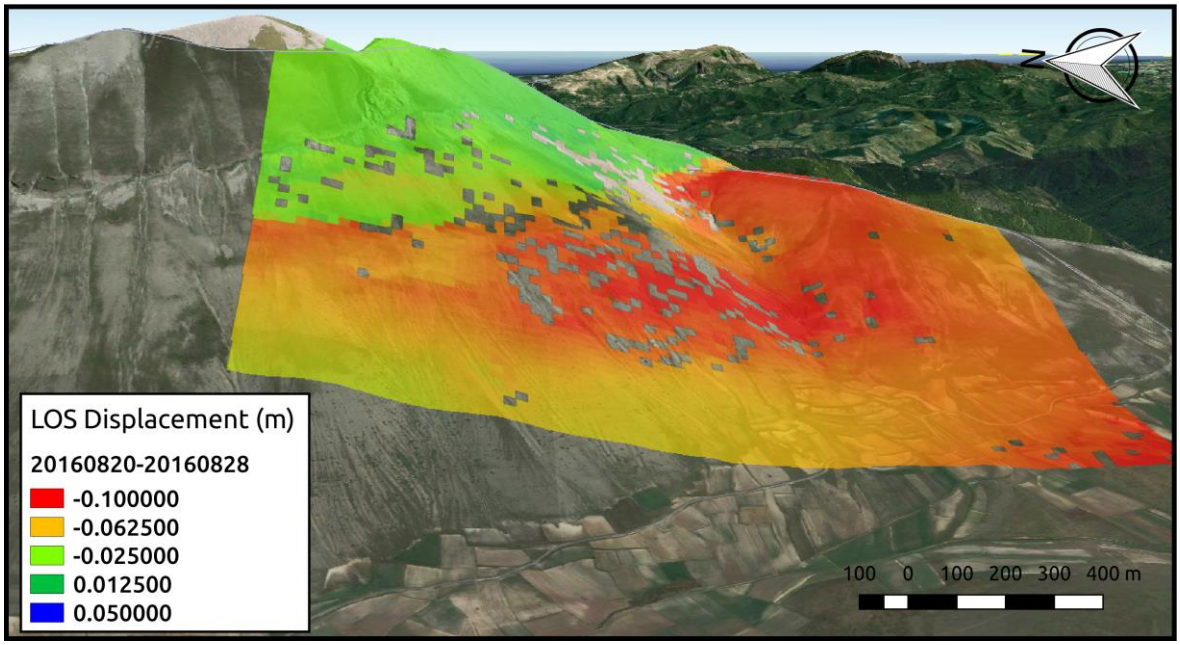

Figure 3: 3D displacement occurred along the flank of Mt. Vettore.

<u>Bolognola</u>

In this case study, both the capabilities of X- and C-band SAR data were exploited. The X-band data were used to detect the deformation phenomenon located ~25Km NE from the epicenters of Visso and Norcia earthquakes. As previously stated, in the CSK wrapped interferogram, a color cycle represents a deformation of ~ 1.55cm along the satellite LoS, hence 2-3cm of surface deformation is more easily detected with respect to the C-band (Figure 4). Moreover, the StripMap acquisition mode of X-band CSK data ensures higher spatial resolution than the IW mode of C-band S1 data. On the other hand, the latter is less sensitive to decorrelation effects and then it was exploited in the quantitative analysis of the observed phenomenon. In details, Figures 5-A and 5-B show the 2D- and 3D-view of InSAR displacement from S1 data, respectively. They reveal a ~2.5cm localized displacement field along the satellite LoS, maybe due to a landslide moving from NW to SE. The temporal interval covered from S1 acquisitions encompasses both the Visso and the Norcia earthquakes (together with the relatives foreshocks and aftershocks), hence it is not possible to discriminate which of the two events activated the landslide. However, a portion of the larger co-

seismic displacement field due to the Norcia earthquake is clearly visible in the bottom left corner of Figure 5-A, as also highlighted in Figure 1. Based on its greater magnitude with respect to the Visso seismic event, it is most likely that the Norcia earthquake is responsible for the observed phenomenon.

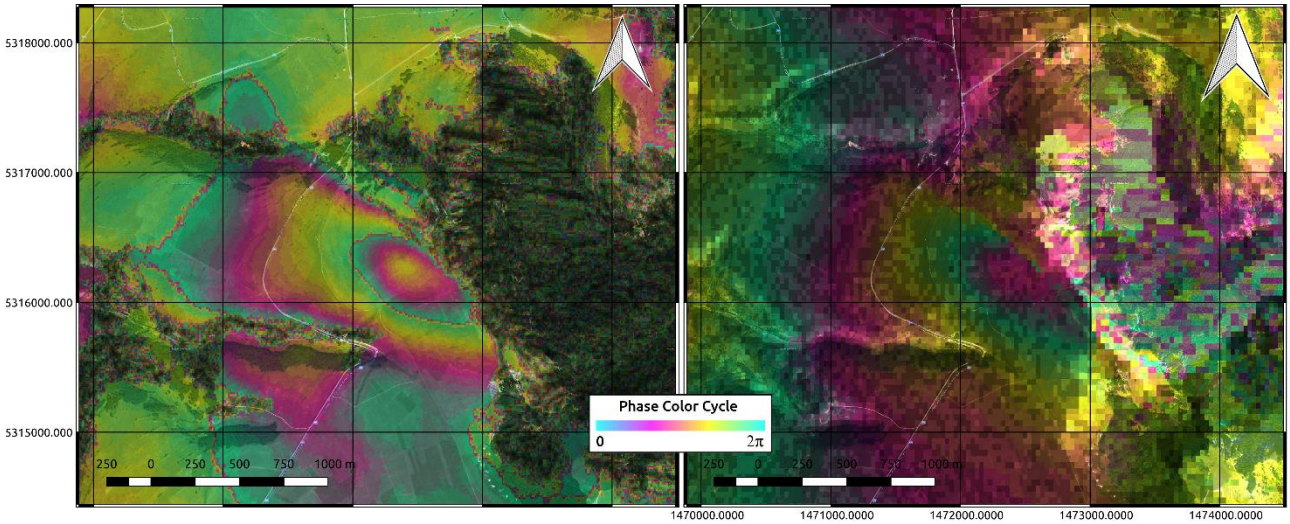

Figure 4: Wrapped interferogram estimated with CSK (left) and S1 (right) data. The smaller wavelength and the higher spatial resolution allow the CSK to better constrain the observed deformation.

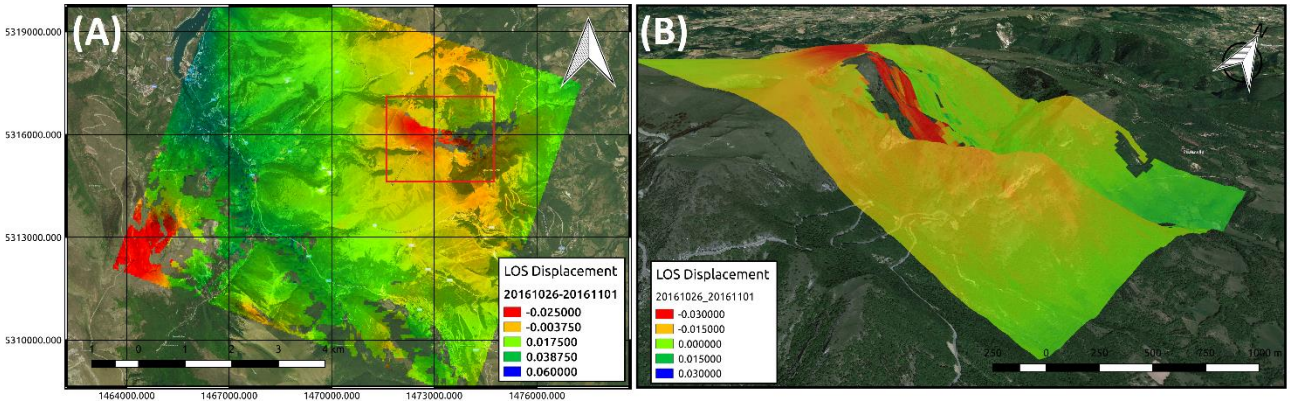

Figure 5: 2D (A) and 3D (B) Displacement map of the *Bolognola* case study estimated by S1 data. The red rectangle highlights the area that is subject to deformation.

Podalla

The Podalla DGSD has already been studied by InSAR data, revealing how the observed area may be prone to significant deformations (Tolomei et al., 2013). In particular, it was found that the Podalla DGSD is a NE-stricking sackung having an NW-dipping sliding plane. Because of its orientation, InSAR data provided along the descending orbit are the most reliable in constraining such a phenomenon. The results of the InSAR analysis are shown in Figure 6. A displacement field with a maximum LoS deformation of ~2-2.5cm is imaged for the Amatrice earthquake as well as for the

Visso and Norcia events. The 3D-view displacement related to the first event, i.e. the August 24th Amatrice earthquake, is also shown in Figure 7 to highlight the interested small-scale area of the observed phenomenon.

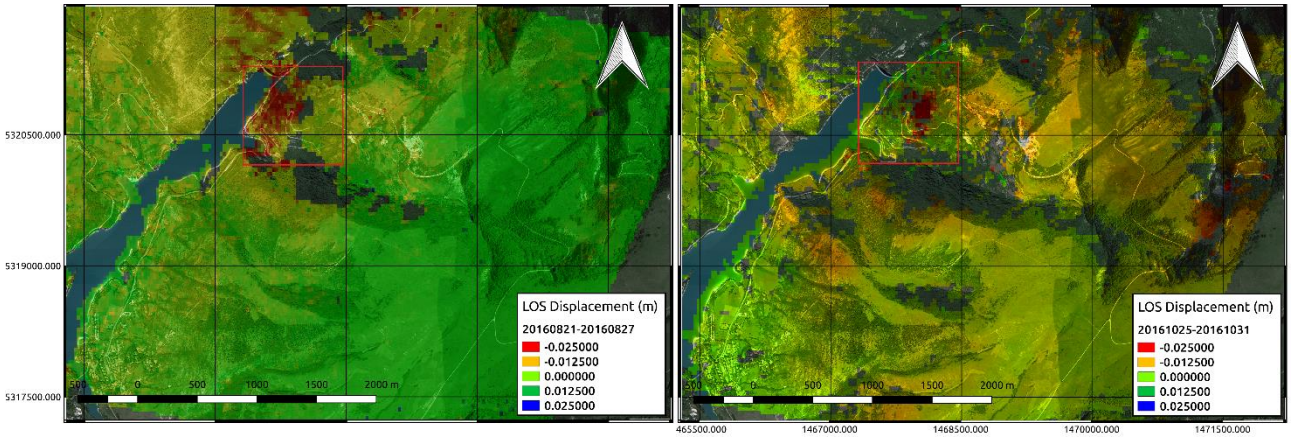

Figure 6: S1 Displacement maps of the Podalla DGSD related to the Amatrice (left) and Visso plus Norcia (right) earthquakes. The DGSD is highlighted in the red rectangles.

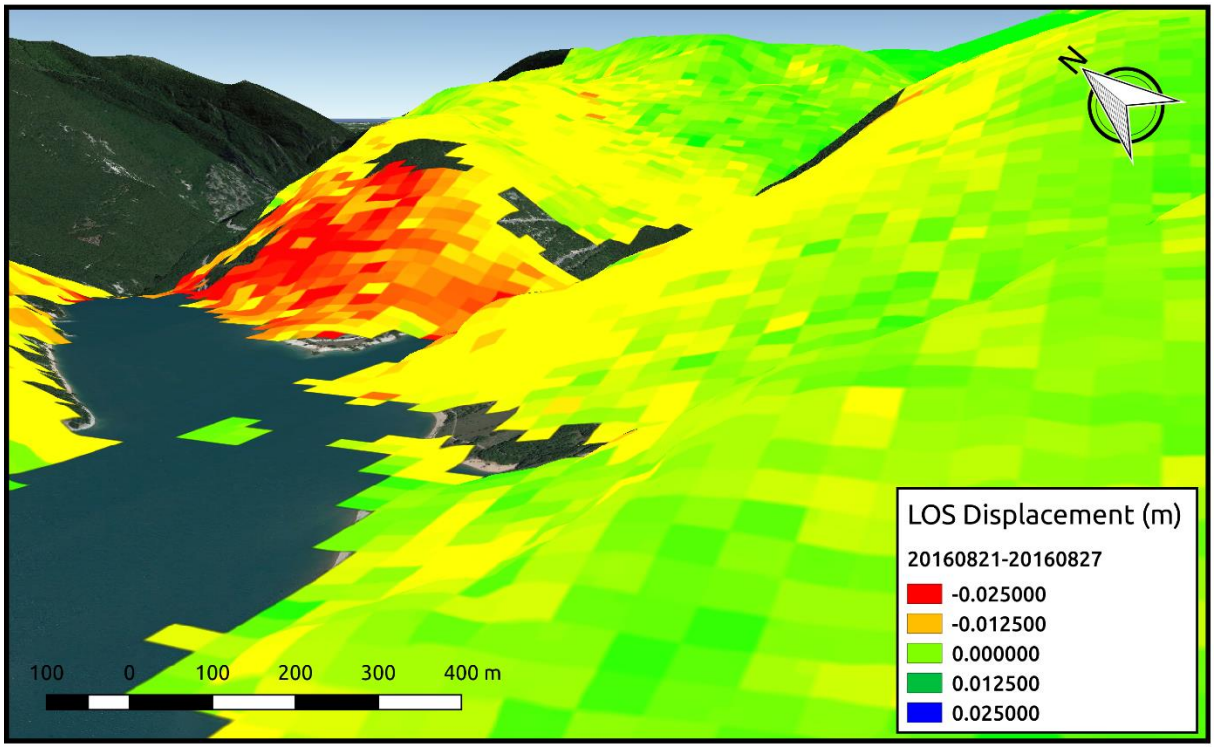

Figure 7: 3D Podalla Displacement map induced by the Amatrice earthquake retrieved by S1 descending data.

Actually, the Podalla DGSD seems be activated by the main first three events of the 2016-2017 Central Italy seismic sequence, i.e. the Amatrice, Visso and Norcia earthquakes. In particular, the cumulative LoS displacement induced by the earthquakes on the DGSD would reach ~5 cm.

However, it is not possible to be completely reliable with the retrieved results. In fact, unfortunately InSAR data seem to be significantly affected by artifacts, which are mainly ascribable to the troposphere. Indeed, during the summer season, the water vapor effects induced by the lake are quite significant and could affect the InSAR results. Hence, further analyses are needed in order to assess the outcomes imaged by the InSAR data.

<u>Cicconi</u>

In this case study, the CSK wrapped interferogram was used to identify the area subject to the deformation phenomenon (Figure 8). Indeed, as stated in the previous sections, the X-band data wavelength is more suitable in constraining such a small displacement.

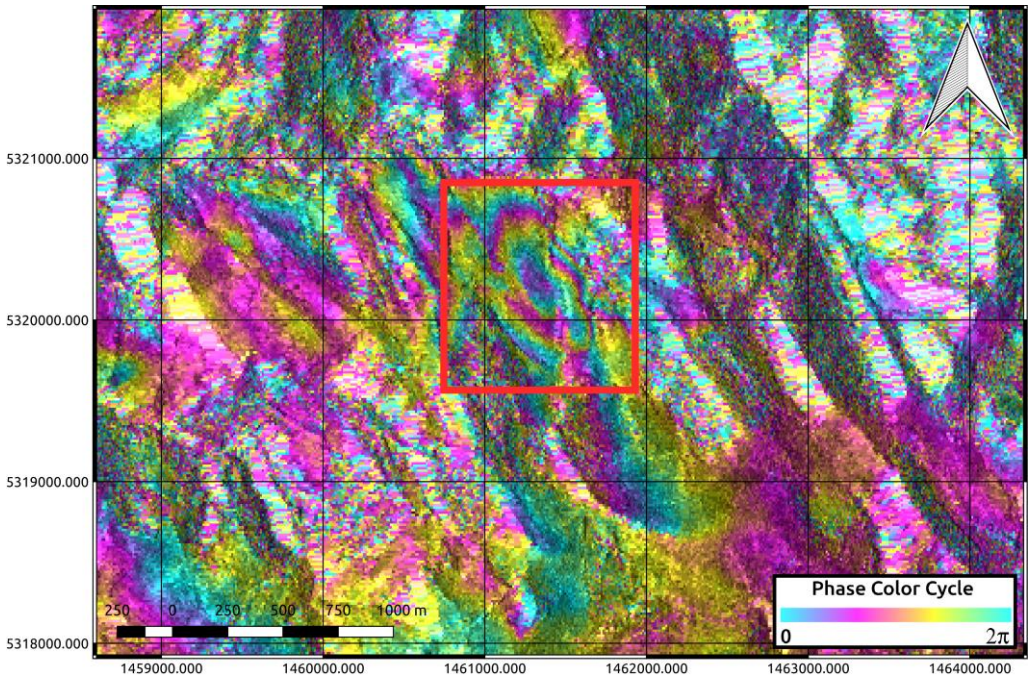

Figure 8: CSK wrapped interferogram showing the fringes of deformation in the *Cicconi* area.

As for the *Mt. Vettore* case study, the S1 InSAR analysis for the entire seismic cycle was conducted (Figure 9). It showed how the area surrounding the *Cicconi* village, in the Fiastra municipality, was affected by a localized deformation of about 2-2.5cm along the satellite LoS (Figures 9-B and 10). This area is located about 25Km NE from the epicenters of Visso and Norcia earthquakes. However, the InSAR outcomes revealed as such a deformation is only due to the October 26th Visso earthquake.

Indeed, the S1 SAR data are able to image separately the two seismic events being acquired on October 21st, October 27th and November 2nd. Then, the detected deformation phenomenon (as well as a part of the displacement field produced by the Visso earthquake) was only observed between October 21st and 27th, as shown in Figure 9-B. On the other hand, the Visso earthquake post-seismic phase (Figure 9-C), that corresponds to the Norcia earthquake co-seismic phase , does not show any deformation in the *Cicconi* area as well as for the pre-seismic phase (Figure 9-A).

The phenomenon is likely due to a landslide activated by the Visso event and slipping from SW to NE as highlighted in Figure 10. Indeed, any movements towards NE are well constrained by InSAR data along ascending orbit. Moreover, the low height of the topography for this area allows minimizing the shadowing and layover effects.

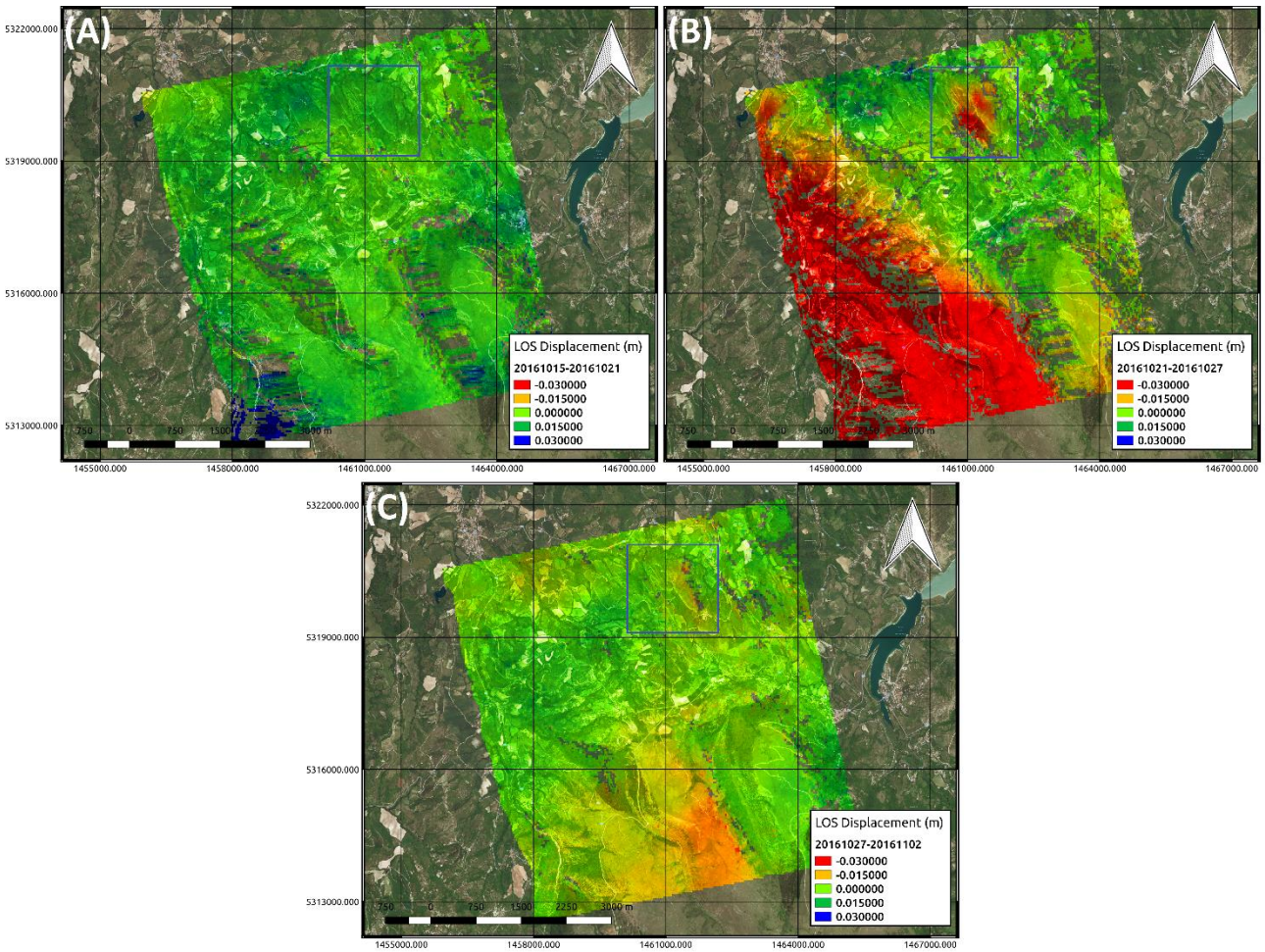

Figure 9: InSAR maps highlighting the effects of the pre-seismic (A), co-seismic (B) and post-seismic (C) phase of the October 26th 2016 Mw 5.9 Visso earthquake. In the blue rectangles the area interested by the deformation.

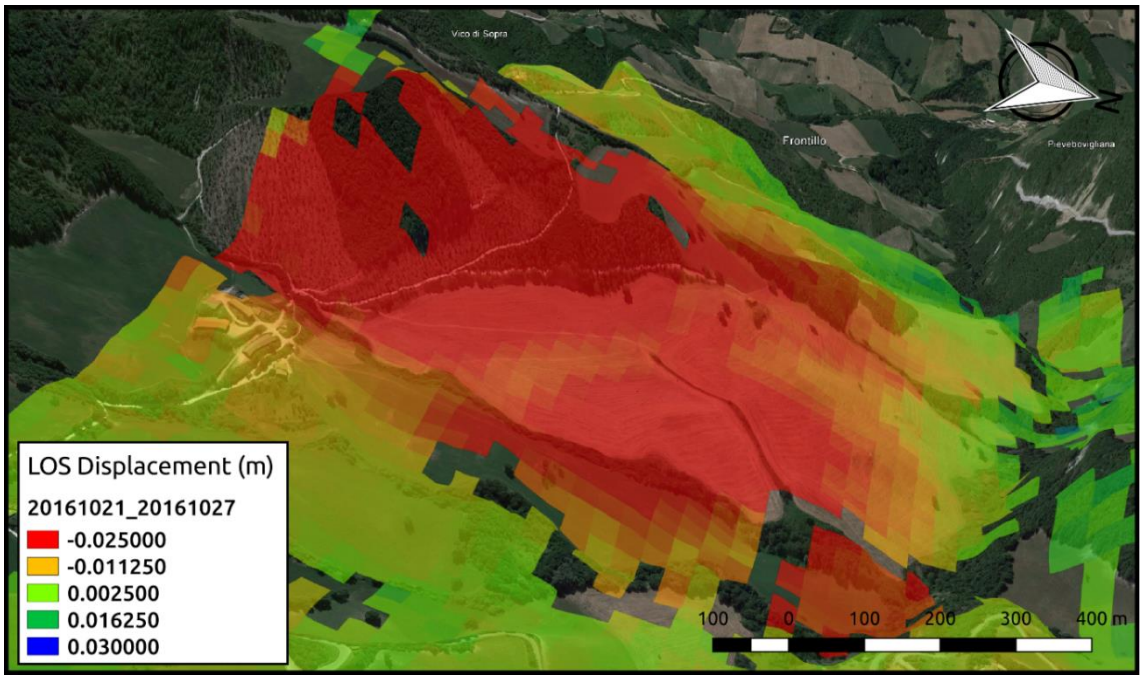

Figure 10: 3D-view of Cicconi displacement induced by the Visso earthquake.

DISCUSSION

The occurrence of a seismic event often leads to important and dangerous consequences for the environment and the human lives. Depending on the location of the epicenter, some local effects induced by an earthquake may occur causing several problems. For example, when an earthquake takes place at sea or near a coastline, it can produce a tsunami that can seriously affect the health of the population and the conformation of the coasts (Alasset et al, 2006; Fritz et al., 2012). If the causative fault is located on the mainland, the local effects mainly depend on the involved scenario. In fact, considering an urban area, the main effect induced by the earthquake is the damage or even the collapse of buildings (Potter et al., 2015). Conversely, within an alluvial valley, an earthquake may produce surface flooding and soil liquefaction phenomena, as highlighted for the 2012 Emilia earthquake (Chini et al., 2015). Lastly, landslides and avalanches are the most important effects induced by seismic events in mountainous areas (Rodriguez et al., 1999).

Obviously, according to the morphology and geology of the scenario, all or some of these effects can occur simultaneously, thus increasing the destructive power of an earthquake.

This paper focuses on the local effects induced by the 2016-2017 Central Italy seismic sequence, in the mountainous areas surrounding the epicenters of the earthquakes. Indeed, this sequence occurred in a sector of the Central Apennine, i.e. the Appennino Umbro-Marchigiano, mainly interesting the massif of the Monti Sibillini among the districts of Ascoli Piceno, Macerata and Perugia. Therefore many local effects, such as landslides or avalanches, were induced in this area by the sequence itself. In this work, InSAR data acquired by X-band CSK and C-band S1 sensors were exploited to detect and analyze local deformations caused by the sequence in 4 different areas of Monti Sibillini: *Monte Vettore*, *Cicconi*, *Podalla* and *Bolognola*. Displacement fields on the order of few centimeters were retrieved by InSAR analysis along the satellite LoS, which were most likely associated to landslide phenomena. Although Central Italy is characterized by rugged topography often leading to atmospheric artifacts on InSAR data, it is possible to be rather confident about the reliability of the retrieved results. Indeed, for the *Monte Vettore* case there are some field evidences confirming the occurrence of the observed phenomenon and previous works were already focused on this topic [Albano et al., 2016; Aringoli et al., 2016]. Concerning the *Bolognola* and *Cicconi* case studies, both X-band CSK and C-band S1 InSAR data were used. They captured the same pattern although with different resolution and definition, thus providing a cross-validation of the results. Indeed, since the atmospheric artifacts are highly correlated in the space but are characterized by a very low temporal correlation, the combined use of SLC data acquired in different time allows attributing the observed pattern to a ground deformation phenomenon (see also supplementary material). As far as the *Podalla* case study is concerned, it has to be considered carefully. As stated in the previous section, the close Fiastra Lake could produce unwanted water vapor effects and, unfortunately, the CSK data are not available for a cross-validation. However, a similar pattern was observed on two different interferograms, with pairs acquired in different seasons, and, there are also evidences of previous ground movements involving the Podalla DGSD (Tolomei et al., 2013). Therefore, the InSAR outcomes are reasonably compatible with a ground deformation phenomenon.

The observed phenomena are due to the first three main earthquakes of the sequence (as well as their foreshocks and aftershocks), i.e., Amatrice, Norcia and Visso earthquakes. The last earthquake, the Mw 5.5 Montereale event, occurred on January during the winter season, striking an area largely characterized by the presence of snow. The latter makes difficult retrieving information by X- and C-band InSAR data. In this case, the more reliable co-seismic displacement map was estimated by L-band ALOS-2 data, which are less affected by snow and temporal decorrelation problems thank to their longer wavelength (λ=24cm).

CONCLUSIONS

This work demonstrated the capability of InSAR data to detect the (small and local) effects induced by earthquakes especially in mountainous areas. When referring to scenarios with a complex topography, as the one interested by the 2016-2017 Central Italy seismic sequence, it can often be difficult to access some areas and evaluate if they are potentially dangerous for the community. Indeed, many landslides or secondary faults could be activated by an earthquake thus making some areas dangerous for any in situ analysis. In addition, the information provided by a possible Global Positioning System (GPS) network could be not suitable for detecting these localized phenomena.

Within such a context, the InSAR data represent a powerful instrument for supporting the hazard assessment and its rapid mapping, defined as the "*creation of maps, geo-information products and spatial analyses dedicated to providing situational awareness emergency management and immediate crisis information for response by means of extraction of reference (pre-event) and crisis (post-event) geographic information/data from satellite or aerial imagery*" (http://www.un-spider.org/sites/default/files/IWG_SEM_EmergencyMappingGuidelines_A4_v1_March2014.pdf).

InSAR data allow covering large areas in a safe, relatively quick and easy way, describing different and particular features that characterize a very complex co-seismic deformation filed. This can be possible thanks to the joined use of space-borne SAR sensors (e.g., CSK and S1 missions) operating at different bands (e.g., the X- and C-bands) and with different acquisition modes (e.g., Stripmap and

IW). They provide an overview, a "post-event picture", of a crisis situation, which can assist Government Institutions such as the Civil Protection Department for safeguarding and mitigating purposes, as well as search & rescue operations. In detail, referring to the InSAR processing of X-band CSK and C-band S1 SAR data acquired during the 2016-2017 Central Italy seismic sequence, experimental results demonstrated the powerful capabilities of both multi-frequency SAR acquisitions and InSAR processing technique for the identification and characterization of secondary effects induced by earthquakes. On the one hand, they revealed landslide deformation phenomena on the order of some centimeters along the satellite LoS for each observed test area. They allowed to define the displacement patterns for each case study both in space and time, providing a cross-validation of deformation phenomena when co-located multi-band InSAR data are available. Furthermore, they highlighted benefits and constraints of X- and C-band SAR data for observing small- and large-scale displacement fields with different spatial resolutions and accuracies.

ACKNOWLEDGMENTS

Authors thank the European Space Agency (ESA) and the Italian Space Agency (ASI) for providing Sentinel-1 and Cosmo-SkyMed SAR data used in this work, respectively. The authors further acknowledges Japan Aerospace eXploration Agency (JAXA) for the provision of ALOS-2 SAR data used for performing the general map of co-seismic displacements in Figure 1. Moreover, authors thank the entire INGV working group involved in the management of the emergency due to the 2016-2017 Central Italy seismic sequence.

REFERENCES

Albano M., Saroli M., Moro M., Falcucci E., Gori S., Stramondo S., Galadini F., Barba S., (2016). Minor shallow gravitational component on the Mt. Vettore surface ruptures related to MW 6, 2016 Amatrice earthquake. *Annals of Geophysics*, vol. 59, Fast Track 5, DOI: 10.4401/ag-7299.

Alasset P.J, Hébert H., Maouche S., Calbini V., Meghraoui M., (2006). The tsunami induced by the 2003 Zemmouri earthquake (*MW*= 6.9, Algeria): modelling and results. *Geophysical Journal International*, vol. 166, pp. 213-226, DOI: 10.1111/j.1365-246X.2006.02912.x.

Aringoli D., Farabollini P., Giacopetti M., Materazzi M., Paggi S., Pambianchi G., Pierantoni P., Pistolesi E., Pitts A., Tondi E., (2016). The August 24th 2016 Accumoli earthquake: surface faulting and Deep-Seated Gravitational Slope Deformation (DSGSD) in the Monte Vettore area. *Annals of Geophysics*, vol. 59, Fast Track 5, DOI: 10.4401/ag-7199.

Bally, A. W., L. Burbi, C. Cooper, and R. Ghelardoni, (1986). Balanced sections and seismic reflection profiles across the central Apennines. *Memorie Società Geologica Italiana*, 35, 257-310.

Barchi, M.R., Minelli, G., Pialli, G., (1998). The crop 03 profile: a synthesis of results on deep structures of the Northern Apennines. *Memorie Società Geologica Italiana*, pp. 383-400.

Barchi, M.R., Galadini, F., La Vecchia, G., Messina, P., Michetti, A.M., Per uzza, L., Pizzi, A., Tondi, E., & Vittori, E., (2000). Sintesi delle conoscenze sulle faglie attive in Italia centrale. CNR-GNDT.

Bignami C., Tolomei C., Pezzo G., Guglielmino F., Atzori S., Trasatti E., Antonioli A., Stramondo S., Salvi S., (2016). Source identification for situational awareness of August 24th 2016 central Italy event. *Annals of Geophysics*, vol. 59, Fast Track 5, DOI: 10.4401/AG-7233.

Cheloni D., Serpelloni E., Devoti R., D'Agostino N., Pietrantonio G., Riguzzi F., Anzidei M., Avallone A., Cavaliere A., et al., (2016). GPS observations of coseismic deformation following the 2016, August 24, Mw 6 Amatrice earthquake (central Italy): data, analysis and preliminary fault model. *Annals of Geophysics*, vol. 59, Fast Track 5, DOI: 10.4401/ag-7269.

Cheloni, D., et al. (2017), Geodetic model of the 2016 Central Italy earthquake sequence inferred from InSAR and GPS data, *Geophysical Research Letters*, 44, doi:10.1002/2017GL073580.

Chiarabba, C., et al., (2009). The 2009 L'Aquila (central Italy) Mw 6.3 earthquake: main shock and af-tershocks. *Geophysical Research Letters* 36, 1–6.

Chini M., Atzori S., Trasatti E., Bignami C., Kyriakopoulos, C., Tolomei C., Stramondo S., (2010). The 12 May 2008 (M 7.9) Sichuan Earthquake (China): Multi-frame ALOS – PALSAR DInSAR Analysis of Coseismic Deformation. *IEEE Geoscience and Remote Sensing Letters*, vol. 7, no. 2, DOI: 10.1109/LGRS.2009.2032564.

Chini M., Albano M., Saroli M., Pulvirenti L., Moro M., Bignami C., Falcucci E., Gori S., Modoni G., Pierdicca N., Stramondo S., (2015). Coseismic liquefaction phenomenon analysis by COSMO-SkyMed: 2012 Emilia (Italy) earthquake. *International Journal of Applied Earth Observation and Geoinformation*, vol.39, pp.65-78, DOI: /10.1016/j.jag.2015.02.008.

Costantini M., (1998). A novel phase unwrapping method based on network programming. *IEEE Transactions on Geoscience and Remote Sensing*, vol. 36, pp. 813-821, DOI: 10.1109/36.673674.

D'Agostino, N., Mantenuto, S., D'Anastasio, E., Giuliani, R., Mattone, M., Calcaterra, S., Gambino, P., Bonci, L., (2011). Evidence for localized active extension in the central Apennines (Italy) from global positioning system observations. Geology 39, 291–294.

Devoti, R., Esposito, A., Pietrantonio, G., Pisani, A.R., Riguzzi, F., (2011). Evidence of large scale deformation patterns from GPS data in the Italian subduction boundary. Earth Planet. Sci. Lett. 311, 230–241.

EMERGEO W.G.:, Pucci S., De Martini P.M., Civico R., Nappi R., Ricci T., Villani F., Brunori C.A., Caciagli M., Sapia V., et al., (2016). Coseismic effects of the 2016 Amatrice seismic sequence: first geological results. *Annals of Geophysics*, vol. 59, Fast Track 5, DOI: 10.4401/ag-7195.

Fritz H., Phillips D., Okayasu A., Shimozono T., Liu H., Mohammed F., Skanavis V., Synolakis C., Takahashi T., (2006). The 2011 Japan tsunami current velocity measurements from survivor videos at Kesennuma Bay using LiDAR. *Geophysical Research Letters*, vol.39, issue 7, DOI: 10.1029/2011GL050686.

Goldstein R., Werner C., (1998). Radar interferogram filtering for geophysical applications. *Geophysical Research Letters*, vol. 25, pp. 4035-4038, DOI: 10.1029/1998GL900033.

Lavecchia, G., Pialli, G., (1980). Appunti per uno schema strutturale dell'appennino Umbro Marchigiano. 2) La copertura. St. Geol. Cam. 6, 23-30.

Lavecchia, G., Brozzetti, F., Barchi, M., Menichetti, M., Keller, J.V.A., (1994). Seismotectonic zoning in east-central Italy deduced from analysis of the Neogene to present deformations and related stress fields. Geological Society of America Bulletin, pp. 1107-1120.

Mariucci, M.T., Montone, P., Pierdominici, S., 2010. Present-day stress in the surroundings of 2009 L'Aquila seismic sequence (Italy). Ge-ophys. J. Int. 182, 1096–1102.

Masi A., Santarsiero G., Chiauzzi L., Gallipoli M.R., Piscitelli S., Vignola L., Bellanova J., Calamita G., Perrone A., Lizza C., Grimaz S., (2016). Different damage observed in the villages of Pescara del Tronto and Vezzano after the M6.0 August 24, 2016 central Italy earthquake and site effects analysis. *Annals of Geophysics*, vol. 59, Fast Track 5, DOI: 10.4401/AG-7271.

Massonet D., Rossi M., Carmona C., Adragna F., Peltzer G., Feigl K., Rabaute T., (1993). The displacement field of the Landers earthquake mapped by radar interferometry. *Nature*, vol. 364, pp. 138–142, DOI: 10.1038/364138a0.

Meletti, C., Patacca, E., Scandone P., (2000). Construction of a seismotectonic model: The case of Italy. Pure Appl. Geophys. 157, 11– 35.

Polcari M., Palano M., Fernández J., Samsonov S., Stramondo S., and Zerbini S., (2016). 3D displacement field retrieved by integrating Sentinel-1 InSAR and GPS data: the 2014 South Napa earthquake. *European Journal of Remote Sensing*, vol. 49, pp. 1-13, 2016, DOI: 10.5721/EuJRS20164901.

Potter S., Becker J., Johnson D., Rossiter K., (2015). An overview of the impacts of the 2010-2011 Canterbury earthquakes. *International Journal of Disaster Risk Reduction*, vol. 14, pp.6-14, DOI: 10.1016/j.ijdrr.2015.01.014.

Rodriguez C., Bommer J., Chandler R., (1999). Earthquake-induced landslides: 1980–1997. *Soil Dynamics and Earthquake Engineering*, vol.18, pp.325-346, DOI: 10.1016/S0267-7261(99)00012-3.

Scarsella F., (1951). Un aggruppamento di pieghe dell'Appennino Umbro-Marchigiano. Boll. Serv. Geol. D'Italia 73, 309-320.

Stramondo S., Vannoli P., Cannelli V., Polcari M., Melini D., Samsonov S., Moro M., Bignami C., and Saroli M., (2014). X- and C-Band SAR Surface Displacement for the 2013 Lunigiana Earthquake (Northern Italy): A Breached Relay Ramp?, *Journal of Selected Topics of Applied Remote Sensing*, vol. 7, pp. 2746-2753, DOI: 10.1109/JSTARS.2014.2313640.

Tavarnelli, E., (1999). Normal faults in thrust sheets: pre-orogenic extension, post-orogenic extension, or both? Journal of Structural Geology 1011-1018.

Tolomei C., Taramelli A., Moro M., Saroli M., Aringoli D., Salvi S., (2013). Analysis of the deep-seated gravitational slope deformations over Mt. Frascare (Central Italy) with geomorphological assessment and DInSAR approaches. *Geomorphology*, vol. 201, pp. 281-292, DOI: 10.1016/j.geomorph.2013.07.002.

Wegmuller U., Werner C., (1997). Gamma SAR processor and interferometry software. *ERS symposium on space at the service of our environment*, n. 414, pp. 1687-1692.

LIST OF FIGURE CAPTIONS

- **Figure 1: InSAR LoS overall displacement induced by the 2016-2017 Central Italy seismic sequence. The map was retrieved by L-band ALOS-2 ascending SAR data. From north to south, the displacement fields due to the Visso (black rectangle), Norcia (red rectangle), Amatrice (white rectangle) and Montereale (blue rectangle) earthquakes are shown, respectively. In the same order, the epicenters are indicated as yellow stars. The different color scales used for the displacement range values are due to the different magnitude of seismic events.**

- **Figure 2: InSAR maps highlighting the effects of the pre-seismic (A), co-seismic (B) and post-seismic (C) phase of the August 24th 2016 Mw 6.0 Amatrice earthquake for the Mt. Vettore. Blue rectangle highlights the area interested by the detected deformation.**

- **Figure 3: 3D displacement occurred along the flank of Mt. Vettore.**

- **Figure 4: Wrapped interferogram estimated with CSK (left) and S1 (right) data. The smaller wavelength and the higher spatial resolution allow the CSK to better constrain the observed deformation.**

- **Figure 5: 2D (A) and 3D (B) Displacement map of the *Bolognola* case study estimated by S1 data. The red rectangle highlights the area that is subject to deformation.**

- **Figure 7: 3D Podalla Displacement map induced by the Amatrice earthquake retrieved by S1 descending data.**

- **Figure 8: CSK wrapped interferogram showing the fringes of deformation in the *Cicconi* area.**

- **Figure 9: InSAR maps highlighting the effects of the pre-seismic (A), co-seismic (B) and post-seismic (C) phase of the October 26th 2016 Mw 5.9 Visso earthquake. In the blue rectangles the area interested by the deformation.**

- **Figure 10: 3D-view of Cicconi displacement induced by the Visso earthquake.**